Fluidized bed with a rotating distributor operated under defluidization conditions

Jesús Gómez-Hernández *, Antonio Soria-Verdugo, Javier Villa Briongos, Domingo Santana

Carlos III University of Madrid, Spain
Energy Systems Engineering Group, Thermal and Fluids Engineering Department, Avda. de la Universidad 30, 28911 Leganés, Madrid, Spain

HIGHLIGHTS

The capability of a rotating distributor to recover a defluidized bed was analyzed.
Defluidization was reached by injecting a punctual volume of water on the bed surface.
Fluidization and recovery processes were analyzed in the time and frequency domain.
An excellent agreement was found for the time and frequency domain results.
The rotating distributor improves the fluidization quality of a defluidized bed.

ABSTRACT

The fluidization conditions of a rotating distributor applied to a 3-D bubbling fluidized bed was studied to assess its potential use as a counteracting measure of defluidization phenomena. The performance of the fluidized bed operating under nominal conditions was characterized for the rotating and the static distributor configuration. Different methods of analysis in the time and frequency domain were applied to establish the performance of the fluidized bed. The frequency domain analysis suggests some kind of local structuring of fluidized bed dynamics imposed by the distributor motion. The punctual injection of water over the surface of the bed lead to a high cohesive wet region that tend to settle down on top of the distributor giving rise to defluidization. The water-induced defluidization tests reflect an improvement of the fluidization quality with the distributor rotation.

Keywords:
Fluidized bed
Liquid injection
Defluidization
Rotating distributor

1. Introduction

Fluidized beds are used for a variety of applications in a wide range of scales, from small chemical reactors to large coal combustors. The injection of gas–liquid jets or liquid jets into gas–solid fluidized beds is encountered in many chemical processes such as fluid coking, fluid catalytic cracking, gas-phase polymerization reactions, and in the production of pharmaceuticals, as a result the particles are covered by liquid layers that might lead to agglomeration phenomena. Although particle aggregation is desired in some processes like granulation, it often poses serious problems leading to defluidization and channeling in many petrochemical operations. Furthermore, other applications, such as fluidized bed combustors (FBCs) or gasifiers (FBGs), also show coating liquid layers. In all cases, uncontrolled liquid phase in a fluidized bed tends to form sticky agglomerates that usually growth until defluidization occurs. If this process is not recognized, it eventually propagates to partial or total defluidization of the system [1].

Many investigations are focused on the mechanisms of formation and distribution of agglomerates inside fluidized beds. The presence of ash might acts as a homogeneous glue layer for the formation of agglomerates in the high temperature zones [2]. In this way, according to Lin et al. [3], the coating layer may be present as liquid phase during combustion. Several researchers have studied the agglomeration or mixing processes after liquid injection in a fluidized bed [4]. Bruhns and Werther [5] suggested that the liquid jet penetrates into the fluidized bed and wets the solids in the vicinity of the nozzle exit, and then, this wet particles become transported into the bed and form agglomerates, which can lead to improper fluidization conditions. Consequently, such "incomplete" fluidization affect the heat and mass transfer rate in fluidized beds, and might lead to local defluidization problems [6–8]. Namely, the larger agglomerates tend to settle down on top of the distributor after being affected by the bed hydrodynamics [9]. These particles in the grid-zone are not much influenced by bubble motion and present the so-called "dead zones" between the holes of the distributor [10,11].

* Corresponding author at: Energy Systems Engineering Group, Thermal and Fluids Engineering Department, Avda. de la Universidad 30, 28911 Leganés, Madrid, Spain. Tel.: +34 916248371; fax: +34 916249430.
E-mail address: jegomez@ing.uc3m.es (J. Gómez-Hernández).

Nomenclature

D	inner diameter of the vessel
E_{WB}	wide band energy
f	frequency
$f_{c,r}$	characteristic frequency with rotating distributor
$f_{c,s}$	characteristic frequency with static distributor
f_n	natural frequency
f_N	Nyquist frequency
Δf	frequency resolution
h_b	fixed bed height
l	lower frequency limit
u	upper frequency limit
U	gas velocity
$U_{mf,s}$	minimum fluidization velocity with static distributor
$U_{mf,r}$	minimum fluidization velocity with rotating distributor
t_r	recovery time

Greek symbols

σ_0	standard deviation of pressure fluctuations under nominal conditions
σ_e	standard deviation of pressure fluctuations during the experiments
σ_n	normalized standard deviation

Abbreviations

COP	coherent-output PSD
IOP	incoherent-output PSD
PSD	power spectral density

Methods for counteracting defluidization phenomena have been recently reviewed in Bartels et al. [1], and use to include operational actions [12,13], changing the fuel supply rate to the process [14] and the use of alternative bed materials [3,6]. Moreover, the improvement of the reactor design by means of the installation of mechanical devices to break the aggregates such as stirring blades has been applied to fight defluidization [15,16]. These studies can be summarized as attempts to modify somehow the gas–solid fluidized bed dynamics trying to overcome defluidization conditions [12]. That is in agreement to the research effort conducted on structuring fluidized bed hydrodynamics [17,18].

It has been previously reported that the rotating distributor motion promotes an increase in the radial dispersion of particles, preventing the temperature gradients by reducing high particle concentration zones present within fluidized beds [19,20]. Furthermore, there is some experimental evidence that the stagnant zones just above the distributor could be broken by the rotating distributor, improving the radial and axial mixing at the bottom of the bed [21]. Therefore, fluidized bed with rotating distributor emerges as a technological solution to be applied in fighting the unwanted defluidization phenomena.

In this paper the rotating distributor motion is presented as an attempt to re-fluidize water induced defluidized system. It is expected that the rotation of the distributor acts over the "dead zones" developed during the "unexpected" defluidization process by breaking the aggregates. Consequently, the distributor rotation effect on the fluidization conditions of a water-induced defluidized bed is studied to assess the potential use of rotating distributor technology as a counteracting measured of defluidization phenomena.

2. Experimental setup

The experiments were carried out in a lab-scale cylindrical Bubbling Fluidized Bed (BFB), equipped with an electrical motor in order to produce a rotation of the distributor. The cylindrical vessel has an inner diameter, D, of 0.192 m, and a height of 1 m. The fixed bed height, h_b, is fixed to two different bed heights with the values of $0.75{\cdot}D$ and $1.5{\cdot}D$.

The rotating distributor was a perforated plate with an open area ratio of 3% and the holes were laid out in a triangular mesh with a pitch of 11 mm. During the experiments, it can be discriminate between rotational distributor case, with an angular velocity of 100 rpm, and the static distributor case, without rotation. This mechanical device (Fig. 1) has been detailed previously [21].

The bed material was silica sand particles, classified as Group B according to Geldart's classification [22]. The particle density was measured to be 2645.5 kg/m^3 with a standard deviation of 2.5 kg/m^3, and a mean diameter of 683 μm. The fluidization airflow had a range of 0–900 l/min and was measured by a rotameter. The set-up is equipped with an air pre-heater of 9000 W capable of maintaining a constant inlet temperature of 30 °C during all the experiments; this was controlled by a PID regulator.

All experiments were carried out in the same facility. The measurement system counts on with 3 pressure local probes with 4 mm of internal diameter and a length of 0.10 m; these dimensions guarantee an undisturbed transfer of the signal [23]. The pressure probes were placed through the wall bed and on the opposite side of the water injection; one probe was placed in the plenum and the other two were placed above the distributor respectively at $0.75{\cdot}D/2$ height and at $0.75{\cdot}D$ height.

Piezoelectric pressure sensors, Kistler type 7261, were connected to the probes to measure the differential pressure fluctuations. The measurements from the Kistler sensors were amplified using a Kistler amplifier type 50,515, which incorporates a low pass filter at 0.16 Hz, and a high pass filter at 200 Hz. The signal was stored in a PC using a National Instruments data acquisition system type 9234 with 4 analog input channels, 24-bit resolution, working at a sampling frequency of 400 Hz.

2.1. Methodology

During the tests the relative fluidization velocity was set to a value of $U/U_{mf,r} = 1.6$, and the fluidized bed was operated at a constant

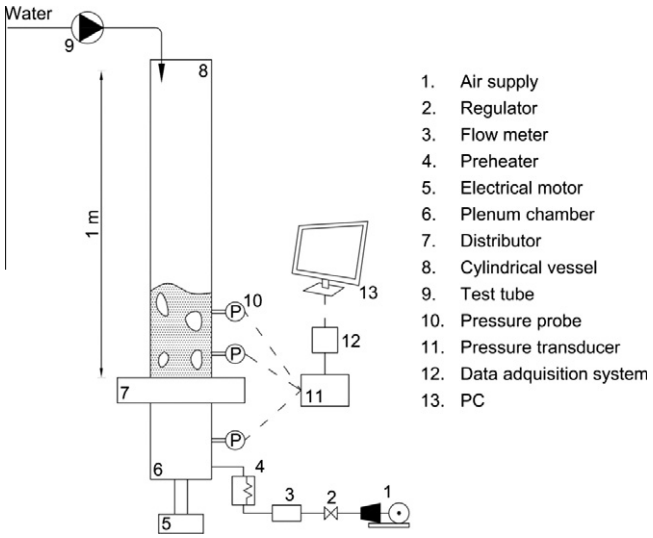

Fig. 1. Schematic diagram of the experimental fluidized bed.

temperature of 30 °C. Those settings are referred as "nominal conditions" and define the steady state operation of the lab-scale fluidized bed, at those conditions there is no presence of agglomerates. The experiments were carried out for two aspect ratios, $h_b/D = 0.75$ and $h_b/D = 1.5$. The minimum fluidization velocity was estimated according to [20,24], being respectively $U_{mf,s} = 0.23$ m/s and $U_{mf,r} = 0.22$ m/s for the static and rotating distributor.

The water injection on the surface of the bed was carried out 1 m above the distributor (perpendicular to it). The volume of water was instantaneously injected using a test tube to spill the water. The same procedure has been used for all the water-induced defluidization tests, starting with the bed running under nominal conditions. Then, water injection starts to cause defluidization. Once the bed is defluidized, different attempts to recover fluidization quality were done using the rotating distributor.

2.2. Water-induced defluidization mechanism

As it is well known, if a liquid is injected in a fluidized bed may spread on the bed particles, increasing their cohesiveness and reducing the bed fluidity. Moreover, choosing water as liquid and silica sand particles as bed material ensured that agglomeration process will occur [25]. Accordingly, the subsequent "wetting" mechanism resulting from the local injection of water on the surface of the fluidized bed assumes that such local injection penetrates into the bed forming a column of wet particles. The column can be described as a large aggregate having a size of the same order of magnitude as the inner diameter of the cylindrical vessel. The wet aggregate defines a sticky region characterized by high cohesive forces which tend to settle down on top of the distributor due to buoyancy effects, improving the development of dead zones over the distributor plate and facilitating the defluidization phenomena. The interparticles forces characterizing those regions are high enough to prevent breakage because of the bubble motion (i.e. channels from distributor to dense phase might cross those regions with no fluidization of wet solids).

3. Method of analysis

The performance of the fluidized bed operating under nominal conditions was characterized for both the rotating and the static distributor. The analysis includes both the time and the frequency domain.

3.1. Time domain analysis

The standard deviation of the pressure signal was employed to analyze the behavior of the bed in the time domain. Despite the standard deviation is strongly influenced by the superficial gas velocity [26], it can be used to monitor the fluidized bed conditions [27]. In this work, at least 5000 samples of pressure fluctuations are statistically required for an accurate characterization of the standard deviation of pressure fluctuations [28]. Moreover, the standard deviation of pressure fluctuations registered during the experiment (σ_e) was normalized dividing by the standard deviation of the nominal case where no water injection was present (σ_0), Eq. (1). This parameter was employed to determine the quality of the fluidization.

$$\sigma_n = \frac{\sigma_e}{\sigma_0} \tag{1}$$

3.2. Frequency domain analysis

Spectral analyses permit to identify the dominant frequencies characterizing the measured pressure fluctuations time-series [29,30]. The power spectral density of the input pressure signal is estimated using averaged modified periodogram method of spectral estimation. Welch's method [31] is used for power spectra estimation with a Hamming window as window function, using the procedure explained by Johnsson et al. [32].

The transient power spectral density was also calculated. It is similar to the power spectrum analysis, but the signal is divided into a number of segments and the power spectral density is calculated for each of them. The process results in a set of spectral densities as a function of time [30]. With this estimation it was possible to identify changes on the frequency in the fluidized bed and to establish the fluidization regime. The parameters used for this method are the same as for the estimation of the power spectral density (PSD), and the frequency range is focused on 0–10 Hz [32].

A method proposed by Van der Schaaf et al. [33] was used to decompose the PSD of pressure time-series into local and global components corresponding to the physical phenomena underlying the pressure time series. That technique provides the measurement of the coherent-output PSD (COP) and the incoherent-output (IOP) of the measured pressure signals by comparing the coherence of the pressure time series collected at the plenum with the pressure signals measured at $0.75 \cdot D/2$. According to [33] the COP provides information of the global behavior of the fluidized bed, whereas local phenomena (i.e. passing gas bubbles), is accounted by the IOP function. In this work, this technique is used to study the rotating distributor effect in the fluidized bed.

The change in energy obtained from the power spectrum reflects a change in operational condition/regime [32]. It is expected that the water and sand mixture present in the experiments is able to modify the dynamic response of the fluidized bed. This energy is estimated using different regions and can be expressed as a function of the total energy of the power spectrum. The ratio between the energy in a region and the total energy is called wide band energy (E_{WB}).

$$E_{WB} = \frac{\sum_l^u Pxx(f)}{\sum_{f=\Delta f}^{f_N} Pxx(f)} \tag{2}$$

In Eq. (2), Δf is the lower spectral frequency, whereas l and u are the lower and upper frequency limits of each region, and f_N is the Nyquist frequency. In the system considered here, three regions are found to divide the wide band energy distribution.

The estimation of the PSD function is conducted by averaging 20 sub-spectra with a frequency resolution ranging between $0.098 \text{ Hz} < \Delta f < 0.049 \text{ Hz}$ as a function of the time series length [32].

4. Results and discussion

The results show the effect of the distributor rotation on the lab-scale bed operated in both under fluidization and defluidization conditions. First of all, the performance of the rotating distributor with the aspect ratio of $h_b/D = 0.75$ is analyzed in frequency domain when the bed is operating at nominal conditions. Later, water-induced defluidization experiments are presented for both aspect ratios ($h_b/D = 0.75$ and $h_b/D = 1.5$) and compared with the reference nominal conditions. The signal used to monitor the rotating distributor effect on the fluidized bed was based on the pressure fluctuation measurements recorded by the sensor placed at the plenum [24,29].

4.1. Nominal characterization

Fig. 2 shows the power spectra of the bed operating under nominal conditions with $h_b/D = 0.75$. A quite similar behavior in the fre-

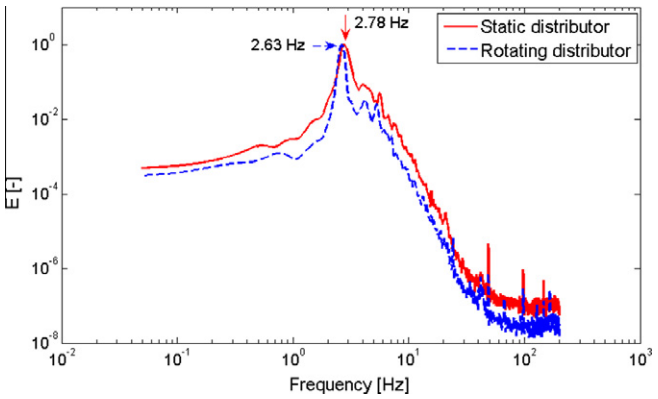

Fig. 2. Power spectra log–log scale, fluidized bed under nominal conditions with $h_b/D = 0.75$.

quency domain is shown for the static and rotating distributor. The dominant frequency of the spectrum for the static distributor is located at $f_{c,s} = 2.78$ Hz, while for the rotating distributor is $f_{c,r} = 2.63$ Hz. These dominant frequencies are very similar to the natural frequency of the fluidized bed estimated according to Baskakov et al. [34], which is $f_n = 2.66$ Hz. Baskakov showed that this natural frequency is related to the gravitational oscillations of the fluidized bed material which rely on pressure waves or fluctuations being generated close to the surface.

The transient spectral density analyses are presented in Fig. 3 for the static and the rotating distributor. The high energy frequencies are represented by hot colors (red[1]) and represent the peak observed in the power spectra (Fig. 2). In contrast, the low energy frequencies are represented by cold colors (blue). These transient spectral density analyses are characteristic of the multiple bubble regime [30]. As expected, the spectrograms were also very similar for both the static and the rotating distributor.

The energy of the power spectrum estimated over the entire frequency domain is a useful parameter to characterize the fluidized bed and can be used to describe different events during fluidization. Fig. 4 presents the cumulative energy plotted in logarithmic axis, which was estimated with Eq. (2), for the static and the rotating distributor. There are three regions on the frequency domain, in the first region ($\Delta f \leqslant f \leqslant 1.3$ Hz) the cumulative energy followed a linear trend and counts on less than the 0.2% of the total energy. The second region contains the 90% of the energy of the signal and was determined from 1.3 Hz to 4.5 Hz. Finally, the third region covered from 4.5 Hz to the Nyquist frequency (200 Hz) with almost the 10% of the energy. According to this division, no meaningful differences were found between the static and the rotating distributor.

In order to show the influence of the rotating distributor on the global and the local phenomenon, COP and IOP functions were estimated. According to that, the power spectrum of the plenum pressure signal is compared with the PSD of the pressure signal measured at $0.75{\cdot}D/2$. The COP analysis, which is generated by global phenomena (Fig. 5a) reflects the effect of the distributor motion in the entire bed. This power spectral density shows the higher peak at 2.53 Hz for the rotating distributor, whereas the static distributor presents a lower COP with a peak at 2.73 Hz. Such frequencies for the rotating and static distributor are close to the corresponding center frequencies characterizing the PSD spectrum shown previously in Fig. 2 ($f_{c,r} = 2.63$ Hz and $f_{c,s} = 2.78$ Hz). The fact that the frequency content characterizing the global behavior of the fluidized bed recorded at the plenum and at $0.75{\cdot}D/2$ position exhibits a high level of coherence means that the distributor is not affecting the downwards compression waves. Therefore, the measurement taken at the plenum can be reliably used to monitor the fluidized bed dynamics either with static or rotating distributor. Nevertheless, the rotating distributor COP spectrum presents higher amplitude than for the static distributor, showing some influence of the rotating distributor on global dynamics.

In contrast the local phenomena accounted by the IOP function exhibits both qualitative and quantitative differences for the rotating and the static distributor (Fig. 5b). For the static distributor case, there is no peak frequency at 2.73 Hz and the corresponding PSD exhibits a uniform distribution of energy among the frequencies. The IOP analysis of the distributor rotation shows three main frequencies, the main peak centered at 1.6 Hz, which correspond to the rotating distributor frequency (100 rpm), a secondary peak centered at 2.73 Hz, that match the major frequency characterizing the COP function, and a third frequency around 4 Hz which also appears in the COP functions (Fig. 5a). Therefore, it is clear that there is a strong influence of the rotating distributor on the local phenomena (e.g. passing bubbles), besides the peak appearing at 1.6 Hz might suggest some kind of local structuring of fluidized bed dynamics imposed by the distributor rotation at 100 rpm. Moreover, for these reasons there are no meaningful differences between the power spectra of the pressure measurements for the fluidized bed with and without the rotating distributor (Fig. 2), due to the local effect of the rotating distributor.

4.2. Punctual injection experiments with $h_b/D = 0.75$

A set of experiments was carried out with a punctual injection of water at the initial time of the experiment, when the fluidized bed was operating under nominal conditions and with the static distributor. Different water volumes were injected on the surface of the bed. Fig. 6 shows the normalized standard deviation of pressure estimated with Eq. (1) for different runs. The chart described the water-induced defluidization process as well as the recovery of the fluidization quality applying the rotating distributor. For all liquid injection tests, the normalized standard deviation presents similar downward trends for 20–30 s after water injection. This time between the liquid injection to defluidization of the bed is defined as the 'defluidization time'. Visual observations confirmed that for the injections of 100 ml, 150 ml and 175 ml, the bed was defluidized after about 30 s of water injection, which is also showed by the normalized standard deviation in Fig. 6. These visual observations led to establish a minimum threshold level value for the normalized standard deviation of 30% under which defluidization was reached. In contrast, after the water injection of 50 ml, visual observations showed that there was a deterioration of the fluidization condition with a decrease of the normalized standard deviation value up to roughly a 60% of the nominal operation condition, however the bed was not defluidized. According to that, a value of 50% has been established for the normalized standard deviation as a threshold to identify the defluidization state.

As Fig. 6 shows, approximately after 2 min of the punctual injection of water, the distributor rotation was started in order to counteracting the defluidization problem and recover the fluidization quality. In the case of 50 ml water injection the rotating distributor tends to recover the fluidization quality easily. For the 100 ml and 150 ml water injection runs, the recovery time, t_r, needed by the normalized standard deviation to reach the defluidization level of $\sigma_n = 50\%$, where the bed is considered to be in fluidized state, is about $t_r = 150$ s for the injection of 100 ml, and $t_r = 200$ s for the injection of 150 ml which match up with visual observations. The rotation of the distributor was therefore found useful to increase the normalized standard deviation over the

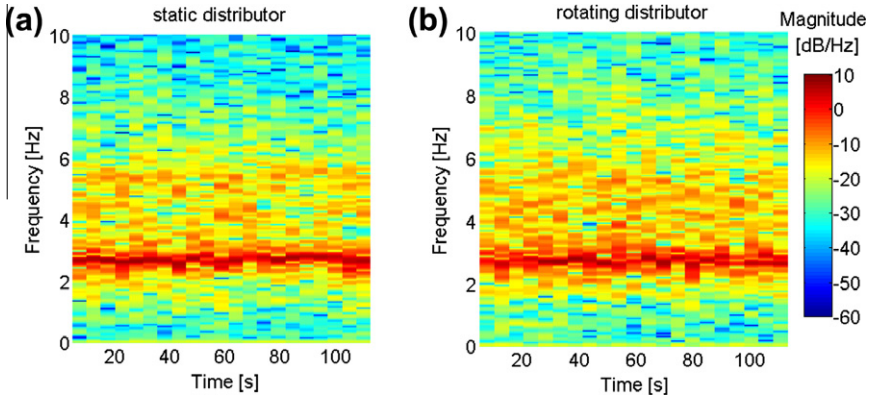

Fig. 3. Transient spectral density for fluidized bed at nominal conditions with $h_b/D = 0.75$. (a) Static distributor. (b) Rotating distributor.

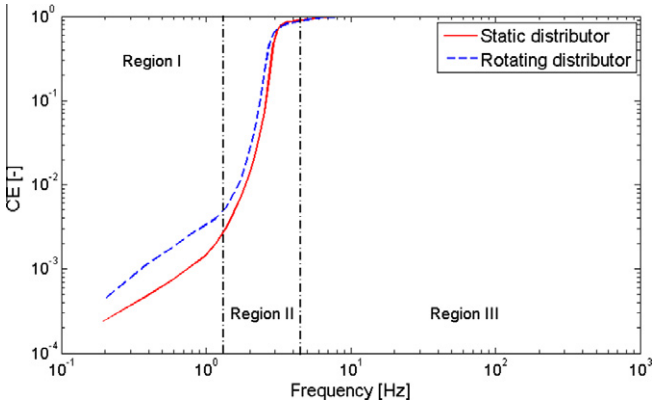

Fig. 4. Cumulative energy of the fluidized bed under nominal conditions with $h_b/D = 0.75$.

threshold for the injections of 100 ml and 150 ml, which indicates an improvement of the fluidization quality. However, for the injection of 175 ml slightly improvements were attained.

The runs showed in Fig. 6, are studied below in the frequency domain by means of the transient PSD (Fig. 7). Accordingly, in Fig. 7a/b can be observed that after the water addition of 50 ml and 175 ml, the characteristic frequencies of the fluidized bed located around the center frequency value, $f_{c,s}$, were gradually losing energy during the defluidization process. Such energy loss is dramatically increased when the wet aggregates settle down on top of the distributor (Fig. 7). It is assumed that the defluidization process starts at the moment at which the characteristic frequency of the fluidized bed begins to disappear. The time of defluidization beginning estimated with the transient PSD of pressure signal match up with the previous threshold of $\sigma_n = 50\%$ established by visual inspection for the normalized standard deviation. Thus, by comparison between Figs. 6 and 7b, it can be confirmed for instance that after the water-injection of 175 ml, the defluidization start at 30 s (characteristic frequency disappearance), which is roughly the same time necessary by the normalized standard deviation to decrease below the threshold level of $\sigma_n = 50\%$ (Fig. 6). Moreover, once the wet aggregates reach the distributor plate and the fluidized bed behaves as a more cohesive system, channeling appears giving rise to pressure fluctuation time series characterized by frequencies values around 8 Hz (Fig. 7b).

Fig. 7a obtained for the punctual injection of 50 ml confirmed the result shown in Fig. 6. Thus as a consequence of the water injection there is some peak frequency dissipation, however the main frequency characterizing the nominal operation conditions is still present in the spectrogram since the bed is not defluidized. Consequently, though the presence of the wet aggregates modified the dynamic transient response of the bed, the bubble motion prevents the wet aggregates to reach the distributor plate hindering the defluidization process.

Once the bed was defluidized, the distributor rotation was switched on. The bubbles were then more homogenously distributed [20] as a consequence of the local structuring of fluidized bed dynamics imposed by the distributor motion at 100 rpm, and the dead zones between holes over the distributor are subse-

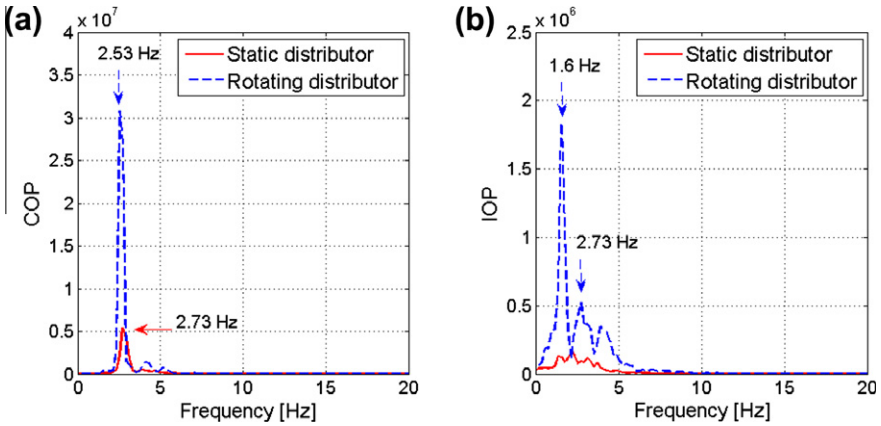

Fig. 5. Fluidized bed working under nominal conditions with $h_b/D = 0.75$. (a) COP. (b) IOP.

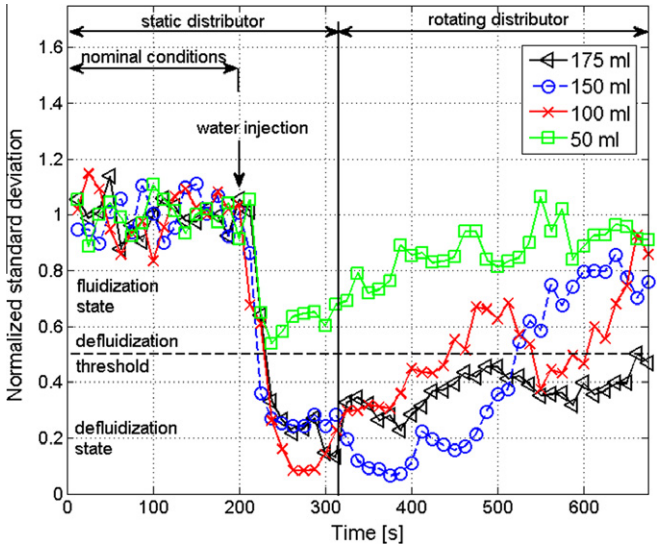

Fig. 6. Normalized standard deviation of pressure after punctual injections of water with $h_b/D = 0.75$.

quently broken improving the radial and axial mixing at the bottom of the bed [21]. Therefore, now the wet regions can be removed from the bottom by the bubble motion facilitating the drying and breakage of the aggregates. The recuperation process (Fig. 7c) shows that the re-fluidization time was about $t_r = 200$ s for the 150 ml injection, which is in agreement to the value estimated previously through the time domain analysis. Such spectrogram (Fig. 7c) is similar to that obtained for the water-injection of 100 ml. Moreover, as the bed dries up, the characteristic bed frequency $f_{c,r}$ gain spectral energy. In agreement to previous result reported in literature [13], the recovery time estimated either by the time domain or frequency domain is much lower than the 10 min needed to re-fluidize the bed with the static distributor.

The spectrogram analysis is also able to show gradual changes in the dynamic of the fluidized bed. In this way, Fig. 7b shows the bed completely defluidized, 30–120 s, with the presence of channels. In addition, in Fig. 7c the stages followed by the system, which go from defluidization between 0 s and 150 s, to gradual fluidization from 150 s to 200 s are shown. Furthermore, the rotation frequency of 1.6 Hz is also present in Fig. 7c from 0 s to 200 s, when the bed was defluidized.

Finally for the 175 ml injection, Fig. 7d shows that no re-fluidization conditions were achieved and a high energy frequency appeared at 1.6 Hz, which corresponds to the rotation of the distributor at 100 rpm. This result is confirmed with the normalized standard deviation in Fig. 6. After defluidization by water injection of 175 ml, rotating effect was small and the bed was vaguely re-fluidized during the test duration.

Based on the results showed in the spectrograms (Fig. 7), the changes produced in the frequency domain clearly affect the energy distribution accounted by the wide band energy method. Fig. 8 presents the energy in each of the regions of the PSD function defined previously in Fig. 4 versus the volume of water injected.

The fluidized bed operating at nominal conditions presents almost the same energy distribution with the static and the rotating distributor as explained before (Fig. 4). It can be observed in Fig. 8a that the punctual injection of 50 ml modified the energy distribution by decreasing around 10% of the energy contained in Region II (E_{WB2}) and transferred it to higher frequencies, Region III (E_{WB3}). This means that the increase of the bed material cohesiveness is reflected at high frequencies (Region III). Such energy distribution is similar to that presented after the injection of 100 ml, but in this case, the defluidization is reached due to the greater amount of water injected. Following the tendency, when the amount of water injected was increased, the energy was transferred from Region II to Region III. The energy contained at low frequencies remained al-

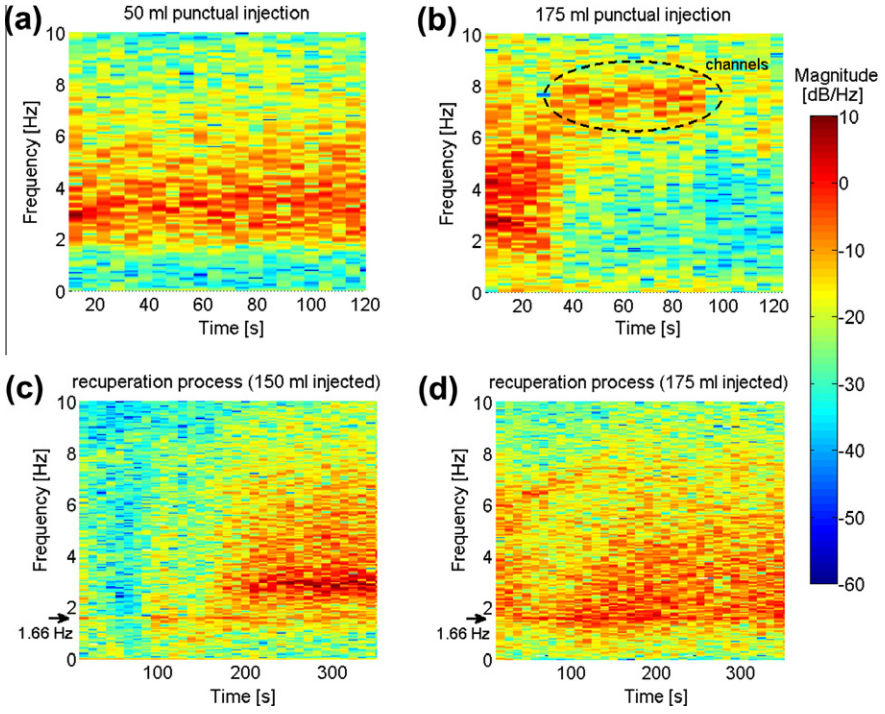

Fig. 7. Transient PSD with $h_b/D = 0.75$. (a) Agglomeration after 50 ml punctual injection. (b) Agglomeration after 175 ml punctual injection. (c) Recuperation after defluidization (150 ml of water). (d) Recuperation after defluidization (175 ml of water).

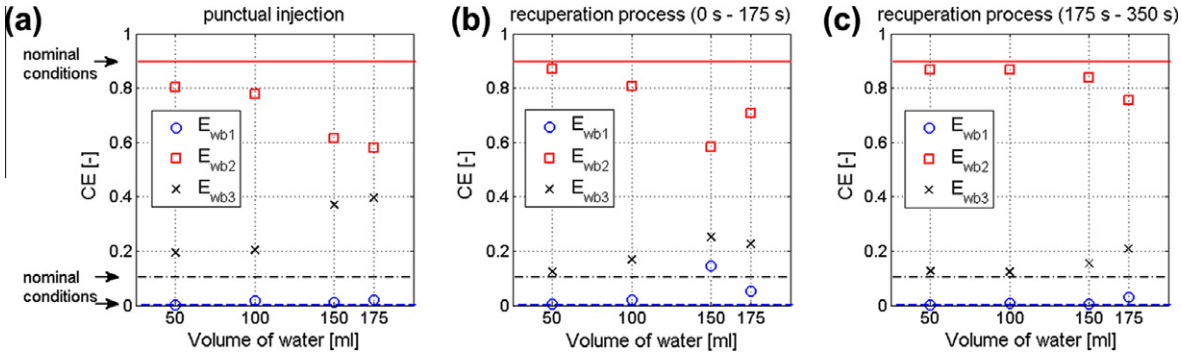

Fig. 8. Wide band energy with $h_b/D = 0.75$. (a) Punctual injection. (b) Recuperation process (0–175 s). (c) Recuperation process (175–350 s).

most constant for the cases in which defluidization was reached. This is explained as a consequence of the appearance of channels around the dead zone, whose formation was explained before.

Based on the re-fluidization time showed in Figs. 6 and 7, the recuperation process is divided to set clearly the energy distribution on the recuperation process, Fig. 8b/c. The signal was divided in two intervals in order to identify more clearly the events caused by the rotating distributor. The defluidized system is considered during the first part, in which the rate of drying was lower. On the second part, the bed is considered to be operated under nominal fluidization conditions, for the 100 ml and 150 ml cases, or near the fluidization, for the 175 ml case.

After the injection of 50 ml, the bed was not defluidized and therefore, the cumulative energy is constant during the recuperation process, Fig. 8b/c. Such energy distribution returns to the values in which there was no liquid. That is, the rotating distributor modifies the energy distribution as a consequence of the change in the structure of the bed. As pointed out by Sobrino et al. [19,20], a more vigorous fluidization can be achieved applying the distributor rotation and also, it promotes an increase in the radial dispersion of the particles, reducing the high water concentration zones present near the injection area. These reasons justified the similar energy distributions of the nominal case and of the results presented before for 50 ml water injection.

However, in the cases in which defluidization was achieved; there are differences between the first and the second half of the recuperation process. During the first part of the experiment (Fig. 8b) the energy of Region III decreased whereas the energy in Region I tend to rise for the cases of 100 ml and 175 ml as a consequence of the distributor rotation. In the case of 150 ml injection, the system suffered a serious defluidization process, which is reflected as an increase in the low frequency region and the corresponding decrease in Region II. On the other hand, the second part of the recuperation process, Fig. 8c, shows that the level of energy has been recover to values approaching the nominal state, were re-fluidization occurred (100 ml and 150 ml). The effect of the rotating distributor improves the fluidization conditions by the breakage of wet aggregates, even in the 175 ml case, which is still poorly fluidized.

4.3. Elimination of the defluidized state for deeper beds

Finally, in this section the counteracting effect of the rotating distributor applied to deep beds is studied, in order to analyze its validity in industrial applications. In this way, the aspect ratio was increased to $h_b/D = 1.5$ in order to analyze whether the bed is recovered or not with and without the rotating distributor. Following the methodology used before, water-induced defluidization experiments for deep beds ($h_b/D = 1.5$) are presented and compared with the results obtained for shallow beds ($h_b/D = 0.75$). Moreover, in these tests for deep beds the volume of water was fixed to 150 ml since it produced a deep defluidization, allowing the recuperation process to occur in a reduced time.

First of all, the fluidization regime of the bed working with $h_b/D = 1.5$ was studied by means of the power spectral density. Fig. 9 compares the PSD of the bed working under nominal conditions with and without the rotating distributor for both aspect ratios. In the case of $h_b/D = 1.5$, the dominant frequency of the

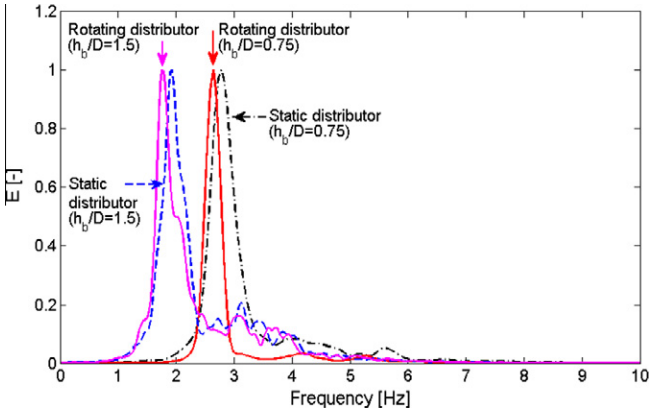

Fig. 9. PSD for $h_b/D = 0.75$ and $h_b/D = 1.5$.

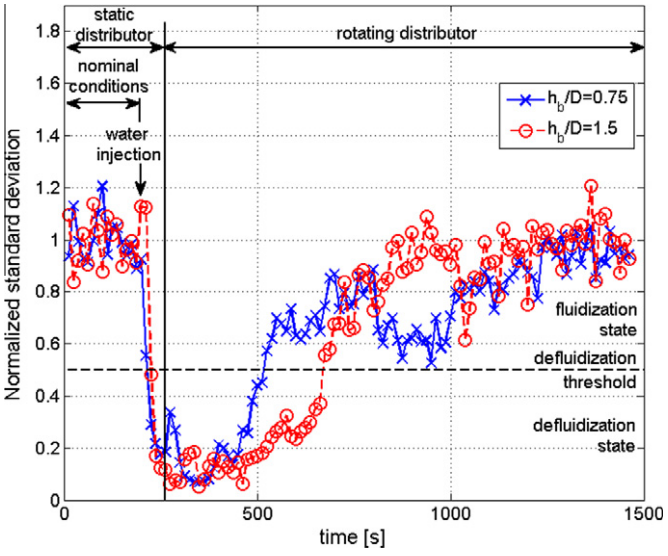

Fig. 10. Normalized standard deviation of pressure for water injection of 150 ml.

spectrum for the static distributor is $f_{c,s}$ = 1.929 Hz, while for the rotating distributor is $f_{c,r}$ = 1.758 Hz. These dominant frequencies are close to the Baskakov frequency, which is f_n = 1.85 Hz, as was the case of h_b/D = 0.75, indicating that the increase of the aspect ratio maintained the single bubble regime for both the static and rotating distributor cases. However, for the deep bed (h_b/D = 1.5) operating with the rotating distributor, a peak appeared at 3.12 Hz which is almost the double of the rotating distributor frequency (1.6 Hz). The presence of that frequency cannot be properly identified with a single process of the fluidization, but might be explained because of the excitation of some dynamic phenomena promoted by the distributor rotation.

Fig. 10 shows the normalized standard deviation for the water-defluidization and recuperation processes studied for h_b/D = 0.75 and h_b/D = 1.5. As can be seen in Fig. 10, the fluidization quality is recovered for both tests by means of the rotating distributor. After water injection, the defluidization time is almost the same for both heights, around 30 s. Once the bed is defluidized, the rotating distributor was switched on after 60 s of water injection in order to break the dead zones and channels. According to the normalized standard deviation, the recovery time is around t_r = 250 s for the shallow bed, whereas for the deep bed it is around t_r = 430 s. This increase in the recuperation time for the deep bed indicate that, as a consequence of the increase in the aspect ratio,

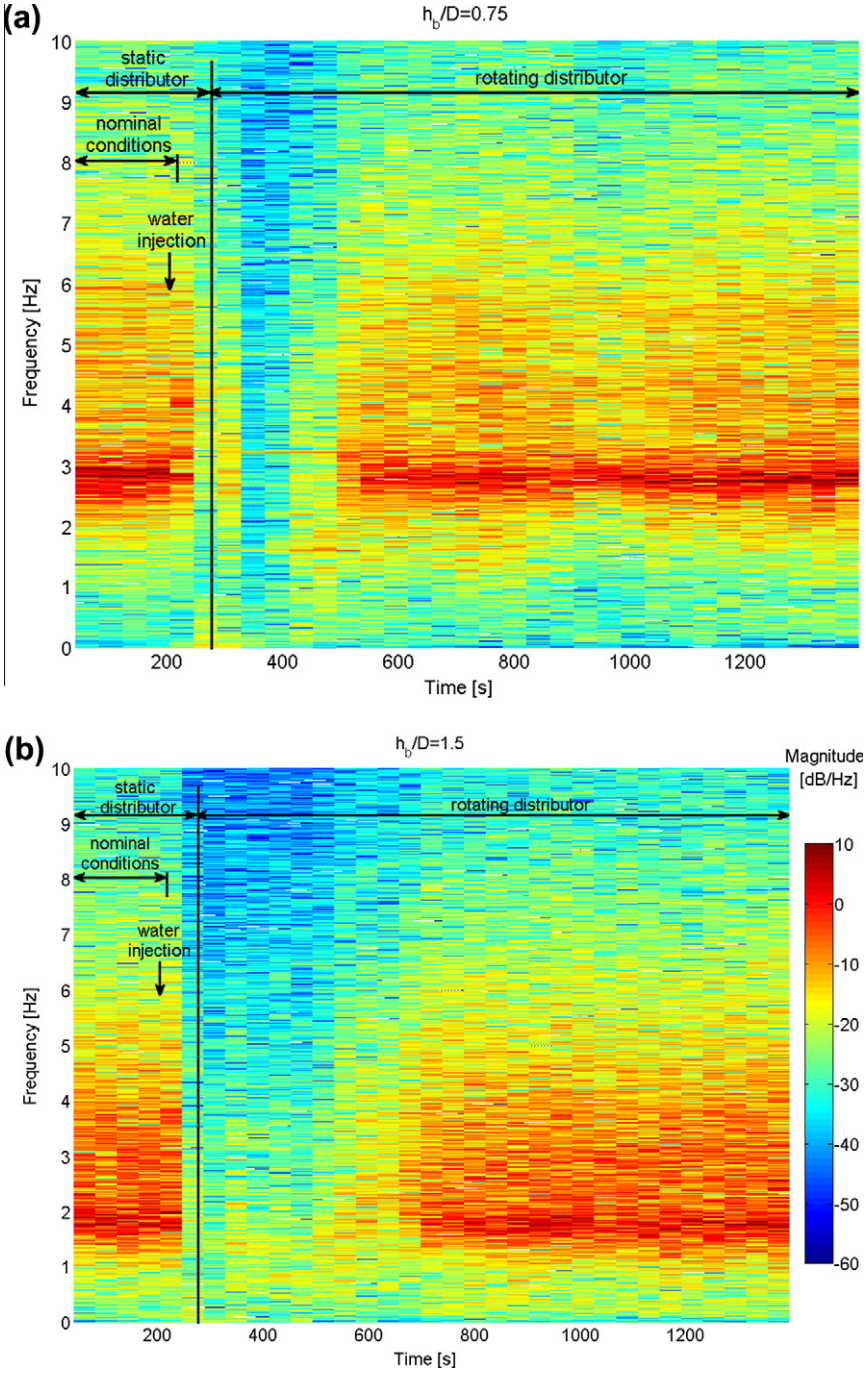

Fig. 11. Transient PSD. (a) h_b/D = 0.75. (b) h_b/D = 1.5.

the presence of slugs reduced the mixing degree of the fluidized bed. Furthermore, that increase of the recuperation time, almost the double comparing both heights, suggests that the mixing degree of the deep bed is inversely proportional to the aspect ratio. In both cases, the local effect of the rotating distributor broke the channels formed close to the distributor improving the fluidization quality. In the case of the shallow bed, there is a smooth decrease on the standard deviation at 700 s after water injection, which was produced by the motion of the wet aggregates. In contrast, the recuperation process of the deep bed follows a gradual recuperation until the bed is properly fluidized. Moreover, in this case ($h_b/D = 1.5$) from 550 s to the end, the significant fluctuations of the standard deviation reflect the decrease of the degree of mixing due to the plug flow regime.

Analyzing the frequency domain with the transient PSD, Fig. 11, the recovery time is found to be close to that showed with the normalized standard deviation. Due to the distributor rotation, the channels were broken and not appeared on the high frequency region for both recuperation processes (Fig. 11). Furthermore, because of that breakage of channels, the normalized standard deviation reflects the evolution of the fluidization quality.

The defluidization time confirmed that the mechanism of defluidization was similar to that described for the $h_b/D = 0.75$ case. However, the effect of the recuperation process with the static distributor might be significant since the increase of the bed height can affect the wet aggregate formation. Moreover, the ratio between the water injected and the bed material is lower with the deep bed than for the $h_b/D = 0.75$ case and the agglomerates can be distributed in a different way affecting the recuperation process. According to that, the wide band energy is estimated in Fig. 12 as a function of time in order to show the energy distribution during the recuperation with the static distributor in which, after water injection, the fluidization quality was tried to recover without the rotating distributor.

In order to estimate properly the wide band energy it is necessary to take into account the energy distribution through the frequency domain since this frequency domain changed with the increase of the bed height, as was shown in Fig. 9. Thus, the frequency ranges that divide the cumulative energy distribution of the fluidized bed working with $h_b/D = 1.5$ under nominal conditions varied to new values, which were used to estimate the wide band energy. Accordingly, the first region was limited between $\Delta f \leqslant f \leqslant 0.8$ Hz, the second region was determined from 0.8 Hz to 4 Hz, and the third region covered from 4 Hz to the Nyquist frequency.

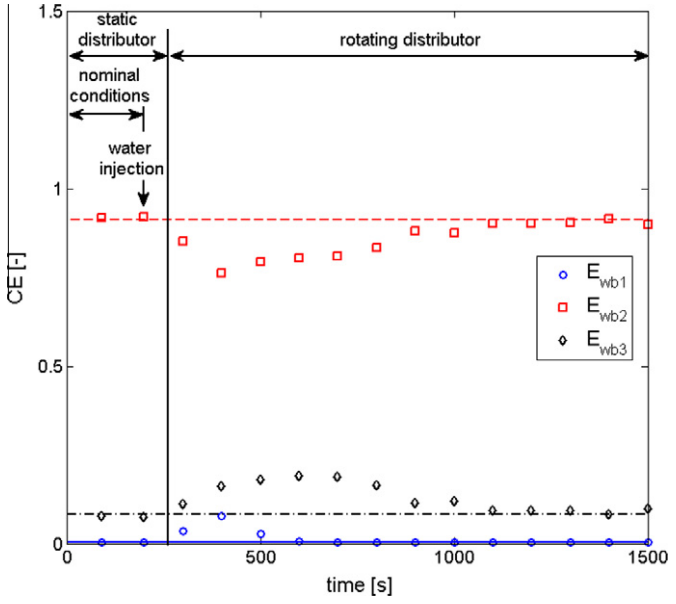

Fig. 12. Wide band energy in function of time after water injection with static distributor ($h_b/D = 1.5$).

Fig. 12 represents the wide band energy estimated each 100 s during the whole test. As can be observed, after water injection there was a decrease on the energy contained in Region II which was transferred to the Region III. This transference of energy was caused by the channels formation near the distributor as a result of the presence of wet aggregates on the dead zones above the distributor. Such a behavior was also shown in the $h_b/D = 0.75$ case (Fig. 8a), but the energy transferred to the Region III was almost 30% in that case, whereas for the $h_b/D = 1.5$ case, the energy transferred only approaches to 10% (Fig. 12).

During the recuperation process with the static distributor presented in Fig. 12, the bed with $h_b/D = 1.5$ can be described as a system having two fluidization zones (upper and bottom bed zones). In the bottom zone, which was located close to the distributor, the channels appeared in the same way that was observed for the $h_b/D = 0.75$ case. Accordingly, the defluidization process occurred and the gas flowed through the channels across that region. However, due to the increase of the bed height, the upper zone apparently did not suffer any defluidization phenomena and consequently the bed was partially fluidized in that upper region, where no channeling appeared. That fact made that the pressure signal measured at the plenum were affected by the compression waves traveling downwards as a consequence of the partial fluidization of the upper region as well as by the channeling process. Consequently, the energy transferred from the Region II to the Region III was limited to a 10%. In the end, the bed was recovered with the static distributor around 900 s after water injection (Fig. 12).

5. Conclusions

The water induced defluidization tests reflect an improvement of the fluidization quality with the distributor rotation. Moreover the frequency domain analysis suggests some kind of local structuring of fluidized bed dynamics imposed by the distributor motion.

During the fluidization with nominal conditions, the fluidized bed operating with the rotating distributor performs near to the Baskakov's frequency, which produced a vigorous fluidization. Furthermore, the distributor rotation had a global effect on the entire bed, promoting the characteristic frequency of the fluidized bed; and also, influenced the local phenomena imposing the rotating frequency of 1.6 Hz. Therefore, rotation of the distributor might be able to introduce a dynamic structure into a gas–solid fluidized bed.

As expected, the punctual injection of water on the surface of the bed with static distributor causes a gradual decrease of the bed fluidization conditions. The distributor rotation has been proved to be able to recover the nominal operational steady state conditions for shallow ($h_b/D = 0.75$) and deep ($h_b/D = 1.5$) beds. Considering all the experiments studied, the recuperation process with the rotating distributor presented a repeatability of 20% according to the recuperation time. The distributor rotation improves the fluidization quality even when the bed was not yet defluidized, at those conditions the aggregate cohesive zones can be moved and subsequently broken during the drying process.

Finally, the proposed methodology of signal analysis used in this work has been proved to detect changes in the dynamic behavior of a fluidized bed. The COP/IOP analyses proved the reliability of the plenum pressure signal. Moreover, the cumulative energy dis-

tribution showed the frequencies of interest during the fluidization, which were used for the wide band energy tool. On the other hand, the frequency domain analyses, such as transient PSD and wide band energy, clearly showed the effect of the defluidization after water injection and allow to identify the quality of the fluidization. Furthermore, both techniques demonstrate that, after water-induced defluidization, the appearance of channels produce a net transfer of energy to higher frequencies within the measured pressure fluctuations signals.

Acknowledgments

The author would like to thank the financial support from Projects DPI2009-10518 (MICINN) and CARDENER-CM (S2009ENE-1660).

References

[1] M. Bartels, W. Lin, J. Nijenhuis, F. Kapteijn, J.R. van Ommen, Agglomeration in fluidized beds at high temperatures: mechanisms, detection and prevention, Prog. Energy Combust. Sci. 34 (2008) 633–666.
[2] M. Ohman, A. Nordin, B.J. Skrifvars, R. Backman, M. Hupa, Bed agglomeration characteristics during fluidized bed combustion of biomass fuels, Energy Fuels 14 (2000) 169–178.
[3] W.G. Lin, K. Dam-Johansen, F. Frandsen, Agglomeration in bio-fuel fired fluidized bed combustors, Chem. Eng. J. 96 (2003) 171–185.
[4] G. Book, K. Albion, L. Briens, C. Briens, F. Berruti, On-line detection of bed fluidity in gas–solid fluidized beds with liquid injection by passive acoustic and vibrometric methods, Powder Technol. 205 (2011) 126–136.
[5] S. Bruhns, J. Werther, An investigation of the mechanism of liquid injection into fluidized beds, AIChE J. 51 (2005) 766–775.
[6] J. Silvennoinen, A new method to inhibit bed agglomeration problems in fluidized bed boilers, ASME Conf. Proc. 2003 (2003) 377–385.
[7] V. Mettanant, P. Basu, J. Butler, Agglomeration of biomass fired fluidized bed gasifier and combustor, Can. J. Chem. Eng. 87 (2009) 656–684.
[8] H.J.M. Visser, S.C. van Lith, J.H.A. Kiel, Biomass ash-bed material interactions leading to agglomeration in FBC, J. Energy Resour. Technol. 130 (2008) 011801.
[9] S. Ariyapadi, D.W. Holdsworth, C.J.D. Norley, F. Berruti, C. Briens, Digital X-ray imaging technique to study the horizontal injection of gas–liquid jets into fluidized beds, Int. J. Chem. Reactor Eng. 1 (2003).
[10] M. Horio, H. Kiyota, I. Muchi, Particle movement on a perforated plate distributor of fluidized-bed, J. Chem. Eng. Jpn. 13 (1980) 137–142.
[11] G. Agarwal, B. Lattimer, S. Ekkad, U. Vandsburger, Influence of multiple gas inlet jets on fluidized bed hydrodynamics using particle image velocimetry and digital image analysis, Powder Technol. 214 (2011) 122–134.
[12] X.S. Wang, M.J. Rhodes, Using pulsed flow to overcome defluidization, Chem. Eng. Sci. 60 (2005) 5177–5181.
[13] A. Ergudenler, A.E. Ghaly, Agglomeration of silica sand in a fluidized-bed gasifier operating on wheat straw, Biomass Bioenergy 4 (1993) 135–147.
[14] A. Nordin, M. Öhman, B.-J. Skrifvars, M. Hupa, Agglomeration and defluidization in FBC of biomass fuels—mechanisms and measures for prevention, in: L. Baxter, R. DeSollar (Eds.), Proceedings of the Engineering Foundation Conference on the Application of Advanced Technology to Ash Related Problems in Boilers, 1995, pp. 353–366.
[15] T. Madhiyanon, A. Lapirattanakun, P. Sathitruangsak, S. Soponronnarit, A novel cyclonic fluidized-bed combustor (Ψ-FBC): combustion and thermal efficiency, temperature distributions, combustion intensity, and emission of pollutants, Combust. Flame 146 (2006) 232–245.
[16] R. Aguado, R. Prieto, M.J. San Jose, S. Alvarez, M. Olazar, J. Bilbao, Defluidization modelling of pyrolysis of plastics in a conical spouted bed reactor, Chem. Eng. Process. 44 (2005) 231–235.
[17] F.K. van Willigen, D. Christensen, J.R. van Ommen, M.O. Coppens, Imposing dynamic structures on fluidised beds, Catal. Today 105 (2005) 560–568.
[18] M.O. Coppens, J.R. van Ommen, Structuring chaotic fluidized beds, Chem. Eng. J. 96 (2003) 117–124.
[19] C. Sobrino, A. Acosta-Iborra, D. Santana, M. de Vega, Bubble characteristics in a bubbling fluidized bed with a rotating distributor, Int. J. Multiphase Flow 35 (2009) 970–976.
[20] C. Sobrino, J.A. Almendros-Ibanez, D. Santana, M. De Vega, Fluidization of Group B particles with a rotating distributor, Powder Technol. 181 (2008) 273–280.
[21] A. Soria-Verdugo, N. Garcia-Hernando, J.A. Almendros-Ibanez, U. Ruiz-Rivas, Motion of a large object in a bubbling fluidized bed with a rotating distributor, Chem. Eng. Process. 50 (2011) 859–868.
[22] D. Geldart, Types of gas fluidization, Powder Technol. 7 (1973) 285–292.
[23] J.R. van Ommen, J.C. Schouten, M.L.M. vander Stappen, C.M. van den Bleek, Response characteristics of probe-transducer systems for pressure measurements in gas–solid fluidized beds: how to prevent pitfalls in dynamic pressure measurements, Powder Technol. 106 (1999) 199–218.
[24] C.A.S. Felipe, S.C.S. Rocha, Prediction of minimum fluidization velocity of gas–solid fluidized beds by pressure fluctuation measurements – analysis of the standard deviation methodology, Powder Technol. 174 (2007) 104–113.
[25] S. McDougall, M. Saberian, C. Briens, F. Berruti, E. Chan, Effect of liquid properties on the agglomerating tendency of a wet gas–solid fluidized bed, Powder Technol. 149 (2005) 61–67.
[26] M. Puncochár, J. Drahos, J. Cermák, K. Selucký, Evaluation of minimum fluidization velocity in gas fluidized beds from pressure fluctuations, Chem. Eng. Commun. 35 (1985) 81–87.
[27] J.R. van Ommen, R.J. de Korte, C.M. van den Bleek, Rapid detection of defluidization using the standard deviation of pressure fluctuations, Chem. Eng. Process. 43 (2004) 1329–1335.
[28] D. Wilkinson, Determination of minimum fluidization velocity by pressure fluctuation measurement, Can. J. Chem. Eng. 73 (1995) 562–565.
[29] M.R. Parise, C.A.M. Silva, M.J. Ramazini, O.P. Taranto, Identification of defluidization in fluidized bed coating using the Gaussian spectral pressure distribution, Powder Technol. 206 (2011) 149–153.
[30] J.R. van Ommen, S. Sasic, J. van der Schaaf, S. Gheorghiu, F. Johnsson, M. Coppens, Time-series analysis of pressure fluctuations in gas–solid fluidized beds – a review, Int. J. Multiphase Flow 37 (2011) 403–428.
[31] P. Welch, The use of fast Fourier transform for the estimation of power spectra, IEEE Trans. Audio Electroacoust. 15 (1967) 70–73.
[32] F. Johnsson, R.C. Zijerveld, J.C. Schouten, C.M. van den Bleek, B. Leckner, Characterization of fluidization regimes by time-series analysis of pressure fluctuations, Int. J. Multiphase Flow 26 (2000) 663–715.
[33] J. van der Schaaf, J.C. Schouten, F. Johnsson, C.M. van den Bleek, Non-intrusive determination of bubble and slug length scales in fluidized beds by decomposition of the power spectral density of pressure time series, Int. J. Multiphase Flow 28 (2002) 865–880.
[34] A.P. Baskakov, V.G. Tuponogov, N.F. Filippovsky, A study of pressure-fluctuations in a bubbling fluidized-bed, Powder Technol. 45 (1986) 113–117.